Proceedings of the 2007 American Control Conference
Marriott Marquis Hotel at Times Square
New York City, USA, July 11-13, 2007

On using the streamwise traveling waves for variance suppression in channel flows

Rashad Moarref and Mihailo R. Jovanović

***Abstract*— We assess the efficacy of using a zero-net-mass-flux blowing and suction in the form of an upstream traveling wave for transition control in channel flows. Our study is motivated by a recent paper by Min *et al.* (J. Fluid Mech., vol. 558) where it was shown that this type of surface actuation yields a sustained sub-laminar drag in a fully developed channel flow. We develop models that govern the dynamics of velocity fluctuations in the presence of stochastic outside disturbances (such as free-stream turbulence and acoustic waves) and show how changes in control parameters affect the fluctuations' kinetic energy density. Effectively, we establish that properly designed streamwise traveling waves can be used to suppress variance of both the streamwise streaks and the Tollmien-Schlichting waves in transitional channel flows.**

***Index Terms*— Flow control; input-output norms; spatially periodic systems; turbulence suppression.**

I. Introduction

An alternative approach to feedback flow control with wall-mounted arrays of sensors and actuators relies on the understanding of the basic flow physics and the open-loop implementation of controls (i.e. without measurement of the relevant flow quantities and disturbances). Examples of the *physics-based sensorless* strategies include: wall geometry deformation such as riblets, transverse wall oscillations, and control of conductive fluids using the Lorentz force. Although several numerical and experimental studies show that *properly designed* sensorless strategies yield a significant drag reduction, an obstacle to fully utilizing these physics-based approaches is the absence of a theoretical framework for their design and optimization.

An enormous potential of sensorless strategies was recently exemplified by [1], where a direct numerical simulation (DNS) study was used to show that a surface blowing and suction in the form of an upstream traveling wave gives a sustained sub-laminar drag in a fully developed channel flow. The underlying mechanism for the sub-laminar drag is the generation of the wall region Reynolds shear stresses of the opposite signs compared to what is expected based on the mean shear. By assuming that a surface actuation *only* influences the velocity fluctuations, Min *et al.* [1] found an explicit solution to the two-dimensional linearized NS equations and showed that the drag is increased with the downstream traveling waves, and decreased with the upstream traveling waves.

An important open question is related to the dynamics of velocity fluctuations in the presence of the streamwise traveling waves. We address this problem by analyzing the variance amplification (i.e., the $\mathcal{H}_2$ norm) of the linearized NS equations in the presence of controls. It is shown that the properly designed surface actuation is capable of suppressing variance of both the streamwise streaks and the Tollmien-Schlichting (TS) waves.

R. Moarref and M. R. Jovanović are with the Department of Electrical and Computer Engineering, University of Minnesota, Minneapolis, MN 55455, USA (e-mails: rashad@umn.edu, mihailo@umn.edu).

Supported in part by the Office of the Dean of the Graduate School of the University of Minnesota Grant-in-Aid of Research, Artistry and Scholarship Award 1546-522-5985.

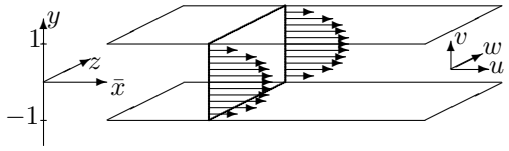

Fig. 1. Three dimensional channel flow.

Our subsequent development is organized as follows: in section II we determine a nominal velocity induced by a blowing and suction in the form of a streamwise traveling wave. In § III, we present an appropriate frequency representation of the linearized NS equations, and briefly discuss a notion of the *ensemble average energy density* of the statistical steady-state. A computationally efficient method for determination of the energy density in the presence of small amplitude traveling waves is described in § IV. In § V, we employ a perturbation analysis to identify the control parameters that suppress variance of the linearized equations. A brief summary of the main results is provided in § VI.

II. Nominal velocity profile

Consider a channel flow governed by the non-dimensional incompressible NS equations

$$\begin{aligned} \mathbf{u}_{\bar{t}} &= -(\mathbf{u}\cdot\boldsymbol{\nabla})\,\mathbf{u} - \boldsymbol{\nabla}P + (1/R)\Delta\mathbf{u} + \mathbf{F}, \\ 0 &= \boldsymbol{\nabla}\cdot\mathbf{u}, \end{aligned} \tag{1}$$

with the Reynolds number defined in terms of maximal nominal velocity $\bar{U}_0$ and channel half-width δ, $R := \bar{U}_0\delta/\nu$. The kinematic viscosity is denoted by ν, the velocity vector is given by $\mathbf{u}$, P is the pressure, $\mathbf{F}$ is the body force, $\boldsymbol{\nabla}$ is the gradient, and $\Delta := \boldsymbol{\nabla}^2$ is the Laplacian. The spatial coordinates and time are represented by $(\bar{x}, \bar{y}, \bar{z})$ and $\bar{t}$, respectively, and the flow geometry is shown in Fig. 1.

Let us assume that in addition to a uniform streamwise pressure gradient the flow is exposed to a zero-net-mass-flux surface blowing and suction in the form of a streamwise traveling wave. In the absence of the nominal body force, $\bar{\mathbf{F}} \equiv 0$, the nominal velocity $\bar{\mathbf{u}} := (U, V, W)$ represents a solution to (1) subject to

$$\begin{aligned} V(\bar{y} = \pm 1) &= \mp 2\,\alpha\,\cos\left(\omega_o(\bar{x} - c\,\bar{t})\right),\ \bar{\mathbf{F}} \equiv 0, \\ U(\pm 1) = V_y(\pm 1) &= W(\pm 1) = 0,\ \bar{P}_{\bar{x}} = -2/R, \end{aligned} \tag{2}$$

where α, ω_o, and c, respectively, denote amplitude, frequency, and speed of the streamwise traveling wave. Positive values of c define a wave moving in the downstream direction while negative values of c define an upstream traveling wave.

The time dependence in $V(\pm 1)$ can be eliminated by the following coordinate transformation $\{x := \bar{x} - c\,\bar{t},\, y := \bar{y},\, z := \bar{z},\, t := \bar{t}\}$. This change of coordinates does not influence the spatial differential operators but it transforms the time derivative to $\partial_{\bar{t}} = \partial_t - c\,\partial_x$, which adds an additional convective term to the NS equations

$$\begin{aligned} \mathbf{u}_t &= c\mathbf{u}_x - (\mathbf{u}\cdot\boldsymbol{\nabla})\,\mathbf{u} - \boldsymbol{\nabla}P + \tfrac{1}{R}\Delta\mathbf{u} + \mathbf{F}, \\ 0 &= \boldsymbol{\nabla}\cdot\mathbf{u}. \end{aligned} \tag{NS}$$

In the new coordinates, (1,2) exhibits a two-dimensional steady-state solution of the form $\bar{\mathbf{u}} = (U(x,y),\, V(x,y),\, 0) := (\Psi_y(x,y),\, -\Psi_x(x,y),\, 0)$, where stream function $\Psi(x,y)$ satisfies the following nonlinear equation

$$\begin{aligned} &\tfrac{1}{R}\Delta^2\Psi + (c - \Psi_y)\,\Delta\Psi_x + \Psi_x\,\Delta\Psi_y = 0, \\ &\Psi(\pm 1) = \pm\tfrac{\mathrm{i}\alpha}{\omega_o}\,(\mathrm{e}^{-\mathrm{i}\omega_o x} - \mathrm{e}^{\mathrm{i}\omega_o x}),\ \Psi_y(\pm 1) = 0. \end{aligned} \tag{SF}$$

The solution to (SF) can be determined numerically using standard NS solvers. In this paper, however, we will consider a situation in which a surface blowing and suction has a small amplitude. For small values of α, we represent $\Psi(x,y)$ as

$$\Psi(x,y) := \Psi_0(y) + \sum_{l=1}^{\infty} \alpha^l \Psi_l(x,y),$$

and perform a perturbation analysis to efficiently solve (SF) and determine corrections to the nominal velocity in the plane channel flow. In the above expansion, $\Psi_0'(y) := \Psi_{0y}(y) = U_0(y) = 1 - y^2$ denotes the plane channel flow, and $\Psi_l(x,y)$ represent the corrections to the nominal stream function caused by the surface blowing and suction. It turns out that $\Psi_l(x,y)$ can be represented as

$$\Psi_l(x,y) = \sum_{r \overset{2}{=} -l}^{l} \Psi_{l,r}(y)\mathrm{e}^{\mathrm{i}r\omega_o x}, \quad l \geq 1,$$

where $\sum_{r\overset{2}{=}-l}^{l}$ signifies that r takes the values $\{-l, -l+2, \ldots, l-2, l\}$. Each $\Psi_{l,r}(y)$ is obtained as a solution to a linear ordinary differential equation which is derived by substituting the expression for $\Psi(x,y)$ in (SF) and matching the terms of equal powers in α. These equations are not presented here due to page constraints and they are to be reported elsewhere.

III. Linearized Navier-Stokes equations

We next present the constitutive equations describing the dynamics (up to a first order) of velocity fluctuations $\mathbf{v} := (u,\, v,\, w)$ around the nominal velocity profile of § II. These equations are obtained by decomposing each field in (NS) into the sum of a nominal and a fluctuating part, e.g. $\mathbf{u} := \bar{\mathbf{u}} + \mathbf{v}$, and by neglecting the quadratic terms in $\mathbf{v}$. A standard conversion to the wall-normal velocity (v)/vorticity (η) formulation removes the pressure from the equations and yields the following evolution model with *forcing*

$$\begin{aligned} E\,\boldsymbol{\psi}_t(x,y,z,t) &= F\,\boldsymbol{\psi}(x,y,z,t) + G\,\mathbf{d}(x,y,z,t), \\ \mathbf{v}(x,y,z,t) &= C\,\boldsymbol{\psi}(x,y,z,t). \end{aligned} \tag{LNS}$$

This evolution model is driven by the body force fluctuation vector $\mathbf{d} := (d_1,\, d_2,\, d_3)$, which can account for the outside flow disturbances such as acoustic waves or free-stream turbulence. These types of excitations are arguably present in most wall-bounded flow configurations and it is of interest to investigate their influence on velocity fluctuations. The internal state of (LNS) is determined by $\boldsymbol{\psi} := (v,\, \eta)$, with Dirichlet and Neumann boundary conditions on v and Dirichlet boundary conditions on η.

All operators in (LNS) are matrices of differential operators in three coordinate directions x, y, and z. We note that operator C in (LNS) captures a kinematic relationship between $\boldsymbol{\psi}$ and $\mathbf{v}$, operator G describes how outside disturbances enter into the evolution model, whereas operators E and F determine internal properties of the linearized equations (for example, stability). While operators E, G, and C do not depend on the nominal velocity, operator F is nominal velocity dependent and, hence, it determines changes in the dynamics due to changes in $\bar{\mathbf{u}}$. For the nominal velocity $\bar{\mathbf{u}} = (U(x,y),\, V(x,y),\, 0)$, F is a 2×2 block-operator with components

$$\begin{aligned} F^{11} &= (1/R)\Delta^2 + ((\Delta U) - (U - cI)\Delta)\partial_x - (\Delta V)\partial_y - \\ &V\Delta\partial_y - 2V_x\partial_{xy} + U_x(\Delta - 2\partial_{xx}) - (\Delta V_y) + (2(\Delta V)\partial_x + \\ &\Delta V_x + V_x(\Delta - 2\partial_{yy}) - 2U_x\partial_{xy})\,(\partial_{xx} + \partial_{zz})^{-1}\partial_{xy}, \\ F^{12} &= -(2(\Delta V)\partial_x + \Delta V_x + V_x(\Delta - 2\partial_{yy}) - \\ &2U_x\partial_{xy})\,(\partial_{xx} + \partial_{zz})^{-1}\partial_z, \\ F^{21} &= -\left(U_y\partial_z + V_x(\partial_{xx} + \partial_{zz})^{-1}\partial_{yyz}\right), \\ F^{22} &= (1/R)\Delta - (U_x + (U - cI)\partial_x + V\partial_y) - \\ &V_x(\partial_{xx} + \partial_{zz})^{-1}\partial_{xy}, \end{aligned}$$

where ∂_x, ∂_y, and ∂_z represent differential operators in x, y, and z, respectively, and $(\partial_{xx} + \partial_{zz})^{-1}$ is defined by

$$(\partial_{xx} + \partial_{zz})^{-1} : f \mapsto g \;\Leftrightarrow\; \left\{ \begin{array}{rcl} f &=& (\partial_{xx} + \partial_{zz})g \\ &=:& g_{xx} + g_{zz}. \end{array} \right.$$

Moreover, for the nominal velocity presented in § II, F inherits spatial periodicity in x from $\bar{\mathbf{u}}$ and each of its components can be represented as

$$F^{ij} = F_0^{ij} + \sum_{l=1}^{\infty} \alpha^l \sum_{r\overset{2}{=}-l}^{l} \mathrm{e}^{\mathrm{i}r\omega_o x} F_{l,r}^{ij},$$

where F_0^{ij} and $F_{l,r}^{ij}$ are spatially invariant operators in the streamwise and spanwise directions.

A. Frequency representation of the linearized model

Owing to the structure of the linearized equations, differential operators E, G, and C are invariant with respect to translations in horizontal directions. On the other hand, operator F is (spatially) invariant in z and (spatially) periodic in x. Thus, the Fourier transform in z can be applied to algebraize the spanwise differential operators. In other words, the normal modes in z are the spanwise waves $\mathrm{e}^{\mathrm{i}k_z z}$, where k_z denotes the spanwise wave number. On the other hand, the appropriate normal modes in x are given by the product of $\mathrm{e}^{\mathrm{i}\theta x}$ and the $2\pi/\omega_o$ periodic function in x, with $\theta \in [0,\, \omega_o)$ [2]. Based on this, each signal in (LNS) (for example, $\mathbf{d}$) can be expressed as

$$\begin{aligned} \mathbf{d}(x,y,z,t) &= \mathrm{e}^{\mathrm{i}k_z z}\mathrm{e}^{\mathrm{i}\theta x}\,\bar{\mathbf{d}}(x,y,k_z,t), \\ \bar{\mathbf{d}}(x,y,k_z,t) &= \bar{\mathbf{d}}(x + 2\pi/\omega_o, y, k_z, t), \end{aligned}$$

with $k_z \in \mathbb{R}$, $\theta \in [0,\, \omega_o)$, where only real parts are to be used for representation of physical quantities. Expressing

$\bar{\mathbf{d}}(x, y, k_z, t)$ in its Fourier series finally yields

$$\begin{aligned} \mathbf{d}(x, y, z, t) \;&=\; \sum_{n=-\infty}^{\infty} \bar{\mathbf{d}}_n(y, k_z, t)\, \mathrm{e}^{\mathrm{i}\theta_n x + \mathrm{i} k_z z}, \\ \theta_n \;&:=\; \theta + n\omega_o, \quad k_z \in \mathbb{R}, \quad \theta \in [0,\, \omega_o), \end{aligned} \tag{NM}$$

where $\{\bar{\mathbf{d}}_n(y, k_z, t)\}_{n \in \mathbb{Z}}$ are the coefficients in the Fourier series expansions of $\mathbf{d}(x, y, k_z, t)$.

The frequency representation of the linearized NS equations is obtained by substituting (NM) into (LNS)

$$\begin{aligned} \partial_t \boldsymbol{\psi}_\theta(y, k_z, t) &= \mathcal{A}_\theta(k_z)\, \boldsymbol{\psi}_\theta(y, k_z, t) + \mathcal{B}_\theta(k_z)\, \mathbf{d}_\theta(y, k_z, t), \\ \mathbf{v}_\theta(y, k_z, t) &= \mathcal{C}_\theta(k_z)\, \boldsymbol{\psi}_\theta(y, k_z, t). \end{aligned} \tag{FR}$$

This representation is parameterized by $k_z \in \mathbb{R}$ and $\theta \in [0,\, \omega_o)$ and $\boldsymbol{\psi}_\theta(y, k_z, t)$ denotes a bi-infinite column vector, $\boldsymbol{\psi}_\theta(y, k_z, t) := \mathrm{col}\,\{\boldsymbol{\psi}(\theta_n, y, k_z, t)\}_{n \in \mathbb{Z}}$. The same definition applies to $\mathbf{d}_\theta(y, k_z, t)$ and $\mathbf{v}_\theta(y, k_z, t)$. On the other hand, for each k_z and θ, $\mathcal{A}_\theta(k_z)$, $\mathcal{B}_\theta(k_z)$, and $\mathcal{C}_\theta(k_z)$ are bi-infinite matrices whose elements are one-dimensional operators in y. The structure of these operators depends on frequency representation of E, F, G, and C in (LNS), and it can be determined using the following set of simple rules [2]:

- A *spatially invariant* operator L with Fourier symbol $L(k_x)$ has a block-diagonal representation

  $$\mathcal{L}_\theta \;:=\; \mathrm{diag}\,\{L(\theta_n)\}_{n \in \mathbb{Z}}.$$

  For instance, if $L = \partial_x$, then $\mathcal{L}_\theta = \mathrm{diag}\,\{\mathrm{i}(\theta + n\omega_o)\}_{n \in \mathbb{Z}}$. Operators E, G, C, F_0, and $F_{l,r}$ in (LNS) are spatially invariant and, thus, their representations are block-diagonal.
- A *spatially periodic function* $T(x)$ with Fourier series coefficients $\{T_n\}_{n \in \mathbb{Z}}$ has a θ-independent block-Toeplitz representation

  $$\mathcal{T} \;:=\; \mathrm{toep}\left\{\cdots, T_2, T_1, \boxed{T_0}, T_{-1}, T_{-2}, \cdots\right\},$$

  where the box denotes the element on the main diagonal of $\mathcal{T}$. For instance, $T(x) = \mathrm{e}^{-\mathrm{i}rx}$ has a block-Toeplitz representation $\mathcal{T} := \mathcal{S}_r$ with only non-zero element $T_{-r} = I$.
- A representation of the sums and cascades of spatially periodic functions and spatially invariant operators is readily determined from these special cases. For example, a matrix representation of operator $\mathrm{e}^{-\mathrm{i}rx}\partial_x$ is given by $\mathcal{S}_r\, \mathrm{diag}\,\{\mathrm{i}(\theta + n\omega_o)\}_{n \in \mathbb{Z}}$.

Based on these, we get the following representations for $\mathcal{A}_\theta$, $\mathcal{B}_\theta$, and $\mathcal{C}_\theta$ in (FR)

$$\begin{aligned} \mathcal{A}_\theta \;&:=\; \mathcal{E}_\theta^{-1}\mathcal{F}_\theta \;=\; \mathcal{E}_\theta^{-1}\mathcal{F}_{0\theta} + \sum_{l=1}^{\infty} \alpha^l \sum_{r \,\overset{2}{=}\, -l}^{l} \mathcal{E}_\theta^{-1}\mathcal{S}_{-r}\mathcal{F}_{l,r\theta} \\ &=:\; \mathcal{A}_{0\theta} + \sum_{l=1}^{\infty} \alpha^l\, \mathcal{A}_{l\theta}, \quad \mathcal{B}_\theta := \mathcal{E}_\theta^{-1}\, \mathcal{G}_\theta, \\ \mathcal{G}_\theta \;&:=\; \mathrm{diag}\,\{G(\theta_n)\}_{n \in \mathbb{Z}}, \quad \mathcal{C}_\theta \;:=\; \mathrm{diag}\,\{C(\theta_n)\}_{n \in \mathbb{Z}}, \end{aligned}$$

where we have used the fact that $\mathcal{E}_\theta := \mathrm{diag}\,\{E(\theta_n)\}_{n \in \mathbb{Z}}$ is an invertible operator. For a convenience of later algebraic manipulations, we rewrite $\mathcal{A}_{l\theta}$ as $\mathcal{A}_{l\theta} := \sum_{r \,\overset{2}{=}\, -l}^{l} \mathcal{S}_{-r}\, \mathcal{A}_{l,r\theta}$ where $\mathcal{A}_{l,r\theta} := \mathrm{diag}\,\{A_{l,r}(\theta_n)\}_{n \in \mathbb{Z}} = \mathrm{diag}\,\{E^{-1}(\theta_{n+r})\, F_{l,r}(\theta_n)\}_{n \in \mathbb{Z}}$. In other words, for a given $l \geq 1$ operator $\mathcal{A}_{l\theta}$ has non-zero blocks only on rth subdiagonals with $r \in \{-l, -l+2, \ldots, l-2, l\}$. This particular structure of $\mathcal{A}_{l\theta}$ is exploited in the $\mathcal{H}_2$ norm perturbation analysis that we present in § IV.

B. Variance amplification of the linearized model

The frequency representation (FR) contains a large amount of information about linearized dynamics. For example, this model can be used to assess stability properties of the underlying nominal flow condition: stability of the linearized system (LNS) is equivalent to the stability of operator $\mathcal{A}_\theta(k_z)$ for each pair (k_z, θ) [2]. However, since the transition in wall-bounded shear flows is not appropriately described by the stability properties of the linearized equations [3]–[8], we perform an input-output analysis of stochastically forced model (FR) to assess the effectiveness of the proposed control strategy. Namely, we set the initial conditions in (FR) to zero and study responses of the linearized dynamics to uncertain body forces. When the body forces are absent the response of stable flows eventually decays to zero. However, in the presence of stochastic body forces the linearized NS equations are capable of maintaining high levels of the steady-state variance [5]–[8]. Our analysis quantifies the effect of imposed streamwise traveling waves on the asymptotic levels of variance and describes how receptivity changes in the presence of control. In § V, we illustrate how this approach can be utilized to provide systematic guidelines for a selection of control parameters.

Let us assume that a stable system (FR) is subject to a zero-mean white stochastic process (in y and t) $\mathbf{d}_\theta(y, k_z, t)$. Then, for each k_z and θ, the *ensemble average energy density* of the statistical steady-state (i.e., the $\mathcal{H}_2$ norm) is determined by

$$\bar{\mathrm{E}}(\theta, k_z) \;=\; \mathrm{trace}\left(\lim_{t \to \infty} \mathcal{E}\,\{\mathbf{v}_\theta(\cdot, k_z, t) \otimes \mathbf{v}_\theta(\cdot, k_z, t)\}\right),$$

where $\mathcal{E}$ is the expectation operator, and $\mathbf{v}_\theta \otimes \mathbf{v}_\theta$ denotes the tensor product of $\mathbf{v}_\theta$ with itself. We note that $\bar{\mathrm{E}}(\theta, k_z)$ determines the asymptotic level of variance maintained by a stochastic outside forcing in (FR). Typically, this quantity is computed by running the DNS of the NS equations until the statistical steady-state is reached. However, for the linearized system (FR), kinetic energy density $\bar{\mathrm{E}}(\theta, k_z)$ can be determined using the solution to the following operator Lyapunov equation [2]

$$\mathcal{A}_\theta(k_z)\mathcal{P}_\theta(k_z) + \mathcal{P}_\theta(k_z)\mathcal{A}_\theta^*(k_z) \;=\; -\,\mathcal{B}_\theta(k_z)\mathcal{B}_\theta^*(k_z), \tag{LE}$$

as

$$\bar{\mathrm{E}}(\theta, k_z) \;=\; \mathrm{trace}\,(\mathcal{P}_\theta(k_z)\, \mathcal{C}_\theta^*(k_z)\, \mathcal{C}_\theta(k_z)),$$

where $\mathcal{P}_\theta(k_z)$ denotes the correlation operator of $\boldsymbol{\psi}_\theta$, that is

$$\mathcal{P}_\theta(k_z) \;:=\; \lim_{t \to \infty} \mathcal{E}\,\{\boldsymbol{\psi}_\theta(\cdot, k_z, t) \otimes \boldsymbol{\psi}_\theta(\cdot, k_z, t)\}.$$

Since $\mathcal{C}_\theta^*(k_z)\, \mathcal{C}_\theta(k_z)$ is an identity operator we have $\bar{\mathrm{E}}(\theta, k_z) = \mathrm{trace}\,(\mathcal{P}_\theta(k_z))$, and the total ensemble average energy is obtained by integration over θ and k_z

$$\begin{aligned} \mathrm{E} \;&=\; \frac{1}{(2\pi)^2} \int_{-\infty}^{\infty} \int_{0}^{\omega_o} \mathrm{trace}\,(\mathcal{P}_\theta(k_z))\; \mathrm{d}\theta\, \mathrm{d}k_z \\ &=\; \frac{1}{(2\pi)^2} \int_{-\infty}^{\infty} \sum_{n=-\infty}^{\infty} \int_{0}^{\omega_o} \mathrm{trace}\,(P_d(\theta_n, k_z))\; \mathrm{d}\theta\, \mathrm{d}k_z \\ &=\; \frac{1}{(2\pi)^2} \int_{-\infty}^{\infty} \int_{-\infty}^{\infty} \bar{\mathrm{E}}(k_x, k_z)\, \mathrm{d}k_x\, \mathrm{d}k_z, \end{aligned}$$

where $P_d(\theta_n, k_z)$ denote elements on the main diagonal of

operator $\mathcal{P}_\theta$, and $\bar{\mathrm{E}}(k_x, k_z) := \mathrm{trace}\,(P_d(k_x, k_z))$. We have arrived at the above expression for E using the fact that $\mathcal{P}_\theta(k_z)$ denotes a frequency representation of a spatially periodic operator, and a simple observation that as n and θ vary over $\mathbb{Z}$ and $[0,\ \omega_o)$, respectively, $k_x = \theta_n = \theta + n\omega_o$ assumes all values in $\mathbb{R}$ [2], [9]. The last expression for the kinetic energy density, i.e. $\bar{\mathrm{E}}(k_x, k_z) := \mathrm{trace}\,(P_d(k_x, k_z))$, is particularly convenient for comparison between the variance amplification of the uncontrolled and controlled flow systems.

IV. Perturbation analysis of variance amplification

Solving (LE) is an arduous undertaking; a discretization of the operators (in y) and truncation of bi-infinite matrices converts (LE) into a large-scale matrix Lyapunov equation. However, since we want to quantify changes in variance amplification with control parameters, as well as with the spatial frequencies, determining even the solution to this approximation to (LE) is computationally expensive. Instead, we employ an efficient perturbation analysis based approach for solving (LE) [9]. This method is well suited for systems with small amplitude spatially periodic terms, and it results in a set of equations with a convenient structure. Namely, the variance amplification can be computed by solving a conveniently coupled system of operator valued Lyapunov and Sylvester equations. A finite dimensional approximation of these equations yields a set of algebraic matrix equations whose order is determined by the size of discretization in y.

Theorem 1: Up to a second order in perturbation parameter α, the ensemble average energy density (variance amplification, $\mathcal{H}_2$ norm) of system (LNS) is given by

$$\begin{aligned}\bar{\mathrm{E}}(k_x, k_z) \;&=\; \mathrm{trace}\,\big(X(k_x, k_z) + \alpha^2 Z(k_x, k_z)\big) \;+\; O(\alpha^4)\\ &=:\; \bar{\mathrm{E}}_0(k_x, k_z) \;+\; \alpha^2 \bar{\mathrm{E}}_2(k_x, k_z) \;+\; O(\alpha^4),\end{aligned}$$

where X and Z solve the following system of Lyapunov and Sylvester equations

$$\begin{aligned}&A_0(\theta_n)\, X(\theta_n) \;+\; X(\theta_n)\, A_0^*(\theta_n) \;=\; -B(\theta_n)\, B^*(\theta_n),\\ &A_0(\theta_{n-1})\, Y(\theta_n) \;+\; Y(\theta_n)\, A_0^*(\theta_n) \;=\\ &-\big(A_{1,-1}(\theta_n)\, X(\theta_n) \;+\; X(\theta_{n-1})\, A_{1,1}^*(\theta_{n-1})\big)\,,\\ &A_0(\theta_n)\, Z(\theta_n) \;+\; Z(\theta_n)\, A_0^*(\theta_n) \;=\\ &-\big(A_{2,0}(\theta_n)\, X(\theta_n) \;+\; X(\theta_n)\, A_{2,0}^*(\theta_n) \;+\\ &A_{1,1}(\theta_{n-1})\, Y(\theta_n) \;+\; Y^*(\theta_n)\, A_{1,1}^*(\theta_{n-1}) \;+\\ &A_{1,-1}(\theta_{n+1})\, Y^*(\theta_{n+1}) \;+\; Y(\theta_{n+1})\, A_{1,-1}^*(\theta_{n+1})\big)\,.\end{aligned}$$

Remark 1: Notation θ_{n-l} in Theorem 1 represents a shortcut for $k_x - l\omega_o$, i.e. $\theta_{n-l} := \theta + (n-l)\omega_o = \theta_n - l\omega_o = k_x - l\omega_o$. Furthermore, in the system of Lyapunov and Sylvester equations for X and Z we have slightly abused the notation by suppressing the dependence on k_z, e.g. $Y(\theta_{n+1}) = Y(\theta_{n+1}, k_z) = Y(k_x + \omega_o, k_z)$.

Remark 2: The expression for the $\mathcal{H}_2$ norm in Theorem 1 can be generalized to account for higher order corrections in α. It turns out that only terms of even powers in α contribute to $\bar{\mathrm{E}}$, which in controlled flows depends on six parameters,

$$\begin{aligned}&\bar{\mathrm{E}}(k_x, k_z, R, \alpha, \omega_o, c) \;=\\ &\bar{\mathrm{E}}_0(k_x, k_z, R) \;+\; \sum_{l=1}^{\infty} \alpha^{2l} \bar{\mathrm{E}}_{2l}(k_x, k_z, R, \omega_o, c).\end{aligned} \tag{ED}$$

Since our objective is to identify trends in variance amplification, we confine our attention to a perturbation analysis up to a second order in α. We briefly comment on the influence of higher order corrections to the $\mathcal{H}_2$ norm in § V, where we show that the trends are correctly predicted by a perturbation analysis up to a second order.

V. Variance amplification in plane channel flow with $R = 2000$

In this section, we study the variance amplification of stochastically excited linearized model. Theorem 1 reveals the dependence of the $\mathcal{H}_2$ norm on the traveling wave amplitude α, for $0 < \alpha \ll 1$. However, since the operators in (FR) depend on the spatial wave-numbers, the Reynolds number R, the wave frequency ω_o, and the wave speed c, the $\mathcal{H}_2$ norm is also a function of these parameters. We discuss how the variance amplification changes with these parameter in plane channel flow with $R = 2000$, and demonstrate that the streamwise traveling waves of properly selected frequency and speed have a potential for reducing the $\mathcal{H}_2$ norm. We also underline some of the basic tradeoffs that need to be addressed in the process of selecting control parameters.

A. Variance amplification of uncontrolled flow

We next briefly comment on the variance amplification in uncontrolled channel flow with $R = 2000$. For an in-depth treatment of this problem we refer the reader to [7], [8].

Fig. 2(a) illustrates the dependence of the uncontrolled $\mathcal{H}_2$ norm on horizontal wave-numbers, $\bar{\mathrm{E}}_0(k_x, k_z)$. The dark red regions signify that the low streamwise wave numbers and $O(1)$ spanwise wave numbers carry most of the uncontrolled flow energy. The largest value of $\bar{\mathrm{E}}_0(k_x, k_z)$ occurs at ($k_x = 0,\ k_z \approx 1.78$), which means that the most amplified structures are infinitely elongated in the streamwise direction and have the spanwise length scale of approximately 3.5δ, where δ is the channel half-width. We note that these input-output resonances do not correspond to the least-stable modes of the linearized equations. Rather, they arise due to the coupling from the wall-normal velocity v to the wall-normal vorticity η. Physically, this coupling is a product of the vortex stretching (vortex tilting, lift-up) mechanism; the nominal shear is tilted in the wall-normal direction by the spanwise changes in v which leads to a transient amplification of η. This mechanism does not take place either when the nominal shear is zero (i.e., $U' = 0$), or when there is no spanwise variations in v (i.e., $k_z = 0$). On the other hand, the least-stable modes of (LNS) create a local peak in $\bar{\mathrm{E}}_0(k_x, k_z)$ around ($k_z = 0,\ k_x \approx 1.2$), with a magnitude significantly lower compared to the magnitude achieved by the dominant streamwise constant flow structures.

Flow structures that contain most variance in uncontrolled plane channel flow with $\{R = 2000,\ k_x = 0,\ k_z = 1.78\}$ are shown in Fig. 2(b). The color plots represent streamwise velocity and the contour lines represent stream function. The most amplified set of fluctuations results in pairs of counter rotating streamwise vortices that generate high and low speed streaks antisymmetric with respect to the channel's centerline. These structures are ubiquitous in both experimental and numerical studies related to transition in channel and boundary layer flows. Thus, it is of interest to design a control strategy capable of weakening the energy content of streamwise constant velocity fluctuations.

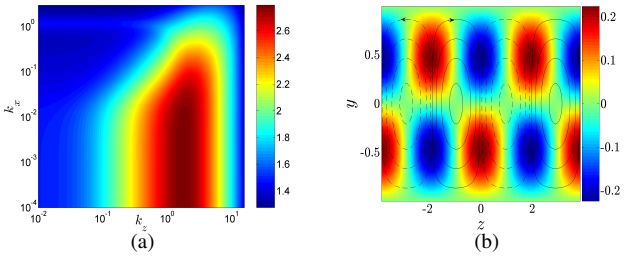

Fig. 2. (a) The $\mathcal{H}_2$ norm $\bar{\mathrm{E}}_0(k_x, k_z)$ in uncontrolled flow with $R = 2000$. The plot is given in the log-log-log scale. (b) Flow structures that contain most variance in uncontrolled flow with $\{R = 2000,\, k_x = 0,\, k_z = 1.78\}$. The color plots represent streamwise velocity fluctuations and the contour lines represent stream function fluctuations.

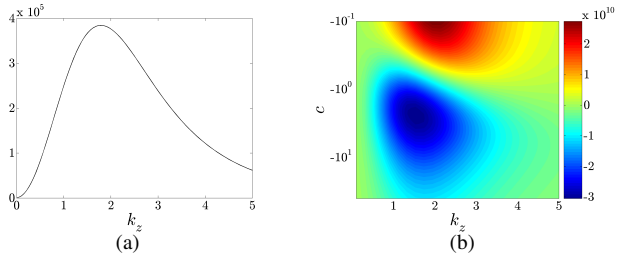

Fig. 3. (a) The $\mathcal{H}_2$ norm $\bar{\mathrm{E}}_0(k_z)$ in uncontrolled flow with $\{R = 2000,\, k_x = 0\}$. (b) The second order correction $\bar{\mathrm{E}}_2(k_z, c)$ to the $\mathcal{H}_2$ norm in controlled flow with $\{R = 2000,\, k_x = 0,\, \omega_o = 0.01\}$.

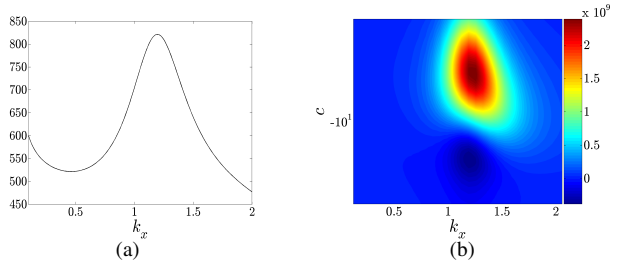

Fig. 4. (a) The $\mathcal{H}_2$ norm $\bar{\mathrm{E}}_0(k_x)$ in uncontrolled flow with $\{R = 2000,\, k_z = 0\}$. (b) The second order correction $\bar{\mathrm{E}}_2(k_x, c)$ to the $\mathcal{H}_2$ norm in controlled flow with $\{R = 2000,\, k_z = 0,\, \omega_o = 0.01\}$.

B. Variance amplification of controlled flow

In this section, we use Theorem 1 to show how blowing/suction in the form of a streamwise traveling wave influences amplification of stochastic outside disturbances in (LNS). We demonstrate that a judicious selection of wave frequency and speed can reduce the $\mathcal{H}_2$ norm. We also discuss some of the basic tradeoffs that need to be considered when selecting control parameters for turbulence suppression.

For a fixed Reynolds number, $\bar{\mathrm{E}}_0$ is just a function of k_x and k_z and it can be easily visualized as in Fig. 2(a). On the other hand, $\bar{\mathrm{E}}_2$ depends on four parameters (k_x, k_z, c, ω_o) which somewhat complicates the visualization process. Here, we analyze the cross-sections of $\bar{\mathrm{E}}_2(k_x, k_z, c, \omega_o)$ by fixing the values of certain parameters. A complete parametric study of the contribution of $\bar{\mathrm{E}}_2$ to the variance amplification will be reported elsewhere.

Since most amplification in the uncontrolled flow occurs at $k_x = 0$, it is relevant to first study the influence of controls on the streamwise constant fluctuations. The uncontrolled $\mathcal{H}_2$ norm at $k_x = 0$ is shown in Fig. 3(a), where we observe a characteristic peak in $\bar{\mathrm{E}}_0(k_z)$ at $k_z \approx 1.78$. This peak determines the most energetic structures in the velocity field excited by a broad-band, stochastic input field $\mathbf{d}$. On the other hand, Fig. 3(b) illustrates the dependence of $\bar{\mathrm{E}}_2$ on k_z and c for the streamwise constant fluctuations with $\omega_o = 0.01$. As evident from this plot, the wave speed c determines whether surface blowing and suction amplifies or attenuates the most energetic components of the uncontrolled flow. We observe the variance attenuation for a fairly broad range of negative wave speeds, with the largest attenuation occurring for upstream traveling waves with $c \approx -2.655$. This value of c represents the wave speed that provides the largest variance suppression (up to a second order in α) of streamwise constant fluctuations in plane channel flow with $R = 2000$ and $\omega_o = 0.01$. On the other hand, the downstream waves and the low speed upstream waves amplify variance of the uncontrolled flow. Note that the largest negative contributions of $\bar{\mathrm{E}}_2$ to the $\mathcal{H}_2$ norm take place in the region of k_z's where function $\bar{\mathrm{E}}_0(k_z)$ peaks. This indicates that the upstream traveling waves introduce resonant interactions with the most energetic modes of the uncontrolled flow. The details of the underlying physical mechanisms that lead to a parametric resonance are deferred to a future study.

The above analysis illustrates the ability of the streamwise traveling waves to weaken the intensity of the most energetic modes of the uncontrolled flow. However, an important aspect in the evaluation of any control strategy is to consider the influence of controls on all of the system's modes. In view of this, we next discuss how control affects the spanwise constant fluctuations and the full three-dimensional fluctuations.

Fig. 4(a) shows the $\mathcal{H}_2$ norm of the uncontrolled flow with $k_z = 0$. The peak in $\bar{\mathrm{E}}_0(k_x)$ at $k_x \approx 1.2$ is caused by the least-stable linearized modes, and the corresponding flow structures (TS waves) carry much less energy than the streamwise constant modes (cf. Fig. 3(a)). Fig. 4(b) shows $\bar{\mathrm{E}}_2(k_x, c)$ for the traveling waves with $\omega_o = 0.01$. Note that the regions with negative and positive contributions to $\bar{\mathrm{E}}$ have changed compared to the streamwise constant case. In particular, the wave speed that provides the largest variance suppression at $k_x = 0$ increases the variance of the TS waves. In order to reduce the energy content of the TS waves the speed of the upstream traveling waves needs to be increased. We observe that $c \approx -20$ provides variance suppression of both streamwise vortices and streaks an the TS waves.

Fig. 5(a) and Fig. 5(b), respectively, show the $\mathcal{H}_2$ norms of the full three-dimensional fluctuations in the uncontrolled and controlled flows with $\{R = 2000, \omega_o = 0.01, c = -20\}$. These plots demonstrate that the properly designed streamwise traveling waves are capable of reducing the energy content of the uncontrolled modes for all k_x and k_z. Furthermore, we observe that the dark red regions (representing large positive values of $\bar{\mathrm{E}}_0$) in Fig. 5(a) almost overlap with the dark blue regions (representing large negative values of $\bar{\mathrm{E}}_2$) in Fig. 5(b). Therefore, the surface blowing and suction reduces the energy density of the uncontrolled flow for wavenumbers where $\bar{\mathrm{E}}_0(k_x, k_z)$ achieves its largest values. Thus, if the perturbation analysis (up to a second order in α) were

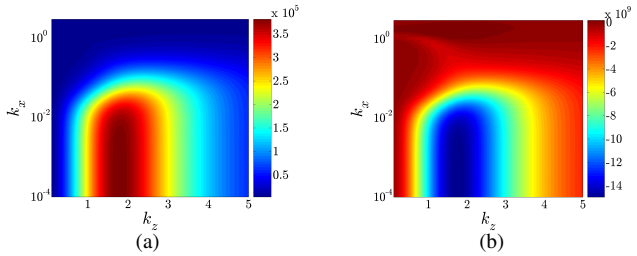

Fig. 5. (a) The $\mathcal{H}_2$ norm $\bar{\mathrm{E}}_0(k_x, k_z)$ in uncontrolled flow with $R = 2000$. (b) The second order correction $\bar{\mathrm{E}}_2(k_x, k_z)$ to the $\mathcal{H}_2$ norm in controlled flow with $\{R = 2000,\ \omega_o = 0.01,\ c = -20\}$.

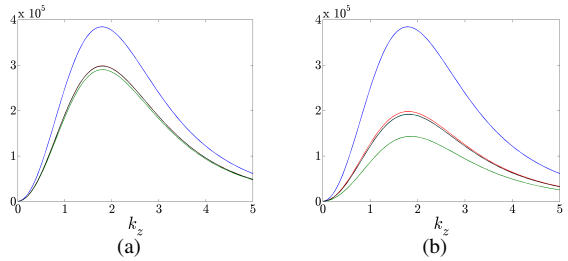

Fig. 6. The $\mathcal{H}_2$ norm $\bar{\mathrm{E}}(k_z)$ in the uncontrolled (blue curve) and controlled flows with $\{R = 2000,\ k_x = 0,\ \omega_o = 0.01,\ c = -20\}$, and: (a) $\alpha = 5/2000$, (b) $\alpha = 8/2000$. The controlled flow plots are obtained by approximating the infinite summations in (ED) by the summations with: 1 (green), 2 (red), 3 (cyan), 4 (magenta), and 5 (black) terms, respectively.

to be used as a basis for the selection of control parameters (in the plane channel flow with $R = 2000$ and $\omega_o = 0.01$), the wave speed $c \approx -20$ would be a reasonable choice. However, we note that the stability of (LNS) will ultimately determine how much α can be increased before destabilizing the equations, which is an important parameter for choosing (α, ω_o, c). The analysis of stability properties is outside the scope of this work.

Fig. 6(a) and Fig. 6(b) show the $\mathcal{H}_2$ norm of the uncontrolled flow (blue curve) with $\{R = 2000,\ k_x = 0\}$, as well as the $\mathcal{H}_2$ norms of the flows subject to the surface blowing and suction in the form of a streamwise traveling wave with $\{\omega_o = 0.01,\ c = -20\}$, $\alpha = 5/2000$ (Fig. 6(a)), and $\alpha = 8/2000$ (Fig. 6(b)). The controlled flow plots are obtained using perturbation analysis by approximating the infinite summations in (ED) by the summations with: one term (green curves), two terms (red curves), three terms (cyan curves), four terms (magenta curves), and five terms (black curves), respectively. Clearly, for selected values of the traveling wave parameters, the approximations of the controlled flow $\mathcal{H}_2$ norms converge in both cases. We note that these results closely match the results obtained using large-scale computations. It is remarkable that the traveling waves of amplitudes equal to only $0.5\,\%$ and $0.8\,\%$ of the maximal nominal velocity ($\alpha = 5/2000$ and $\alpha = 8/2000$) are capable of suppressing the largest variance of the uncontrolled flow by approximately $23\,\%$ and $50\,\%$, respectively. Furthermore, it is noteworthy that the second order correction to the $\mathcal{H}_2$ norm captures the essential trends as to how much variance can be suppressed in the presence of controls.

VI. Concluding Remarks

This paper represents a continuation of recent efforts [10]–[12] to develop a *model-based* approach for a design of *sensorless flow control strategies* in wall-bounded shear flows. The proposed method uses input-output analysis of the linearized NS equations as a basis for a selection of control parameters for variance suppression. The proposed system-theoretic framework avoids the need for the DNS/experiments in the early design stages and is capable of predicting the essential trends in a computationally efficient manner.

The new model-based design paradigm represents a spatial analog of the well-known principle of *vibrational control* [13], where the system's dynamical properties are altered by introducing zero-mean oscillations into the system's coefficients. Depending on the relationship between the natural modes of the uncontrolled system and the forcing frequency, the vibrational control may have a potential for providing stability of the overall system and for changing its input-output norms. For example, it is well known that the inverted pendulum can be stabilized by sensorless means using high frequency oscillations of the suspension point [13]. We show that the principle of vibrational control can be also utilized in systems governing the dynamics of flow fluctuations in channel flows, where coefficients multiplying system's state have spatial periodicity. The key observation is that there is a potential for changing dynamical properties of the linearized NS equations (in favorable or unfavorable manner) whenever controls with spatial and/or temporal periodicity enter into the system's coefficients.

References

[1] T. Min, S. M. Kang, J. L. Speyer, and J. Kim, "Sustained sub-laminar drag in a fully developed channel flow," *J. Fluid Mech.*, vol. 558, pp. 309–318, 2006.

[2] M. Fardad, M. R. Jovanović, and B. Bamieh, "Frequency analysis and norms of distributed spatially periodic systems," *IEEE Transactions on Automatic Control*, 2006, submitted.

[3] K. M. Butler and B. F. Farrell, "Three-dimensional optimal perturbations in viscous shear flow," *Phys. Fluids A*, vol. 4, p. 1637, 1992.

[4] L. N. Trefethen, A. E. Trefethen, S. C. Reddy, and T. A. Driscoll, "Hydrodynamic stability without eigenvalues," *Science*, vol. 261, pp. 578–584, 1993.

[5] B. F. Farrell and P. J. Ioannou, "Stochastic forcing of the linearized Navier-Stokes equations," *Phys. Fluids A*, vol. 5, no. 11, pp. 2600–2609, 1993.

[6] B. Bamieh and M. Dahleh, "Energy amplification in channel flows with stochastic excitation," *Phys. Fluids*, vol. 13, no. 11, pp. 3258–3269, 2001.

[7] M. R. Jovanović, "Modeling, analysis, and control of spatially distributed systems," Ph.D. dissertation, University of California, Santa Barbara, 2004.

[8] M. R. Jovanović and B. Bamieh, "Componentwise energy amplification in channel flows," *J. Fluid Mech.*, vol. 534, pp. 145–183, July 2005.

[9] M. Fardad and B. Bamieh, "A perturbation approach to the H_2 analysis of spatially periodic systems," in *Proceedings of the 2005 American Control Conference*, Portland, OR, 2005, pp. 4838–4843.

[10] M. R. Jovanović, "Turbulence suppression in channel flows by small amplitude transverse wall oscillations," in *Proceedings of the 2006 American Control Conference*, Minneapolis, MN, 2006, pp. 1161–1166.

[11] ——, "Turbulence suppression in channel flows by small amplitude transverse wall oscillations," *Physics of Fluids*, 2006, submitted.

[12] R. Moarref and M. R. Jovanović, "Transition control using an array of streamwise vortices," in *Proceedings of the 45th IEEE Conference on Decision and Control*, San Diego, CA, 2006, pp. 107–112.

[13] S. M. Meerkov, "Principle of vibrational control: theory and applications," *IEEE Trans. Autom. Control*, vol. AC-25, no. 4, pp. 755–762, 1980.